

Article

Structure–Activity Relationship of Aloperine Derivatives as New Anti–Liver Fibrogenic Agents

Kun Wang, Zhihao Guo, Yunyang Bao, Yudong Pang, Yinghong Li *, Hongwei He * and Danqing Song

Institute of Medicinal Biotechnology, Chinese Academy of Medical Sciences and Peking Union Medical College, Beijing 100050, China; kunwang224@163.com (K.W.); guozhihao96@163.com (Z.G.); 17714333891@163.com (Y.B.); pyd101101@163.com (Y.P.); songdanqing@imb.pumc.edu.cn (D.S.)

* Correspondence: liyinghong@imb.pumc.edu.cn (Y.L.); hehwei@imb.pumc.edu.cn (H.H.);
Tel.: +86-10-63-03-30-12 (Y.L.); +86-10-83-16-66-73 (H.H.)

Received: 8 October 2020; Accepted: 26 October 2020; Published: 27 October 2020



Abstract: Twenty-seven novel 12*N*-substituted aloperine derivatives were synthesized and investigated for their inhibitory effects on collagen $\alpha 1$ (I) (COL1A1) promotor in human hepatic stellate LX-2 cells, taking aloperine (**1**) as the hit. A structure-activity relationship (SAR) study disclosed that the introduction of suitable substituents on the 12*N* atom might enhance the activity. Compound **4p** exhibited a good promise on down-regulating COL1A1 expression with the IC₅₀ value of 16.5 μ M. Its inhibitory activity against COL1A1 was further confirmed on both mRNA and protein levels. Meanwhile, it effectively inhibited the expression of other fibrogenic proteins, such as transforming growth factor $\beta 1$ (TGF- $\beta 1$) and smooth muscle actin (α -SMA). It also exhibited good in vivo safety profile with the oral LD₅₀ value of 400 mg kg⁻¹ in mice. The results initiated the anti-liver fibrogenic study of aloperine derivatives, and the key compound **4p** was selected as a novel lead for further investigation against liver fibrogenesis.

Keywords: aloperine; structure–activity relationship; COL1A1; anti-liver fibrogenesis

1. Introduction

Liver fibrosis, as a key pathogenic factor in chronic liver disease progression, is a consequence of chronic damage associated with alcoholic or non-alcoholic fatty liver disease, hepatitis, metabolic or genetic diseases [1,2]. Hepatic fibrosis is characterized by the dysregulated deposition of extracellular matrix (ECM), complexed with progressive destruction of normal liver tissue [2]. Without any treatment, hepatic fibrosis could progress to liver cirrhosis, hepatocellular carcinoma, and even hepatic failure [3]. However, up to now, no effective therapy is available for liver fibrosis except the elimination of underlying etiology or liver transplantation [4,5]. Therefore, the discovery of an effective antifibrotic therapy is still an unmet clinical need.

Transforming growth factor $\beta 1$ (TGF- $\beta 1$), the major fibrogenic cytokine, plays critical roles in the activation of hepatic stellate cells (HSCs) into myofibroblasts [6–10]. Active myofibroblast-like cells are characterized by increased migration, α -smooth muscle actin (α -SMA) expression, and robust collagen production, wherein type I collagen (COL1) constitutes the main source of extracellular matrix (ECM) in clinical and experimental liver fibrosis [11,12]. Taking COL1A1 promotor as the biomarker, a luciferase screening cell model based on the elevation effect of TGF- $\beta 1$ upon the expression of COL1A1 promotor was established earlier in our group [13], and successfully applied to the screening and evaluation of anti-hepatic fibrosis drug candidates [14–16]. The in vivo pharmacodynamics study confirmed that compounds down-regulating the transcription of COL1A1 gene could effectively reverse liver fibrosis in vivo [15].

Aloperine (**1**, Figure 1), an endocyclic quinolizidin alkaloid isolated from the species *Sophora alopecuroides*, has a wide range of biological activities, such as anti-pulmonary fibrosis, anti-cancer, anti-inflammation, anti-virus and so on [17–22]. In view of its unique endocyclic and flexible structural scaffold, as well as a moderate potency in suppressing pulmonary fibrosis, compound **1** was taken as the hit to explore its effect on liver fibrosis. However, the anti-COL1A1 evaluation results indicated that it only held a mild activity by giving inhibitory rate of 4.7% at the concentration of 40 μ M. Therefore, structural modification and optimization on **1** was carried out in this paper in the aim of achieving effective anti-liver fibrogenic leads.

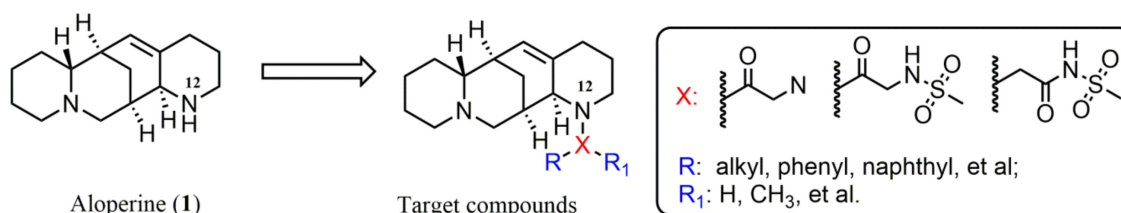


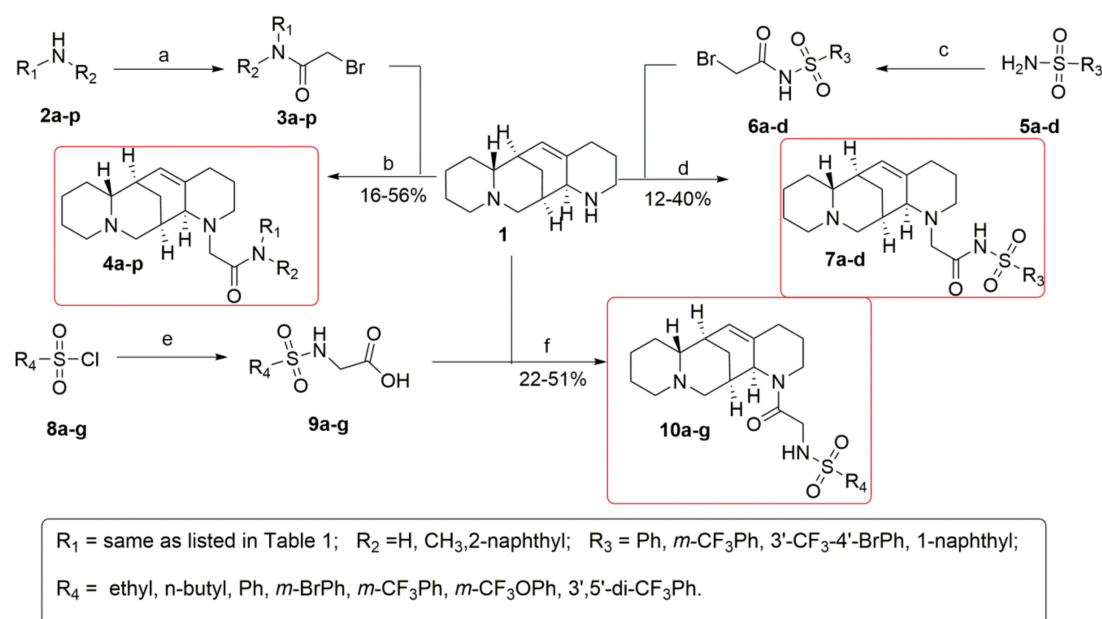
Figure 1. Chemical structure of aloperine and the modification strategy.

In the present study, the anti-COL1A1 structure-activity relationship (SAR) of aloperine derivatives were explored for the first time, and twenty-seven novel aloperine derivatives with structural diversities on the 12N substituents were designed, synthesized and evaluated for their anti-COL1A1 activities.

2. Results and Discussion

2.1. Chemistry

The synthetic routes of all target compounds are depicted in Scheme 1. The target 12N-carbamoylmethyl aloperine derivatives **4a–p** were obtained by alkylation of **1** with the key intermediates **3a–p**, which were synthesized via acylation of bromoacetyl bromide with substituted amines **2a–p** under alkaline conditions [15].



Scheme 1. Reagents and conditions: (a) Bromoacetyl bromide, anhydrous CH₂Cl₂, Et₃N, 0 °C to rt, 2 h; (b) CH₂Cl₂, Et₃N, rt; (c) Bromoacetyl bromide, toluene, reflux, 5 h; (d) K₂CO₃, DMF, heat, 100 °C; (e) Glycine, H₂O, NaOH, 0 °C to rt; (f) HOBt, DIEA, EDCI, anhydrous CH₂Cl₂, rt.

Similarly, the acylation of substituted sulfenamides **5a–d** with bromoacetyl bromide in refluxing toluene afforded the key intermediates **6a–d**, which were alkylated with **1** to achieve the target 12*N*-sulfonylcarbamoylmethyl aloperine derivatives **7a–d** in total yields of 12–40%. At the meantime, glycine was sulfonylated by different sulfonyl chlorides **8a–g** to produce intermediates **9a–g**, and the coupling of **9a–g** with **1** in the presence of EDCI/HOBt formed the target 12*N*-sulfonylaminoacetyl aloperine compounds **10a–g**, in total yields of 22–51%.

2.2. SAR for Inhibition of COL1A1 Promotor of the Target Compounds in Human LX-2 Cells

A single luciferase reporter gene detection model was applied to evaluate the inhibitory effects of all target compounds on the expression of COL1A1 promotor in human hepatic stellate LX-2 cells at the concentrations of 40 and 80 μM , taking EGCG as the positive control [23]. The LX-2 cell lines were transfected with COL1A1 promotor luciferase plasmid pGL4.17-COL1A1P for 24 h, then simultaneously treated with TGF- β 1 and a tested compound for 24 h [13]. The structures and inhibitory effects (%) of all target compounds were shown in Table 1.

Initially, the carbamoylmethyl moiety was selected as the linker, and a series of new 12*N*-carbamoylmethyl aloperine derivatives **4a–p** and **7a–d** with various substitutions were generated and evaluated. The introduction of an alkyl moiety, as in the cases of ethyl (**4a**), tetrahydro-2*H*-pyran-4-yl (**4b**) and 1-adamantyl (**4c**) lead to a slight increase in activity as compared to **1**. Among them, **4c** with a bulky 1-adamantyl group gave the higher activity, indicating that the introduction of a bulky motif might be beneficial for activity. At the meantime, the alkyl moiety was changed into a substituted benzene moiety to provide compounds **4d–l**. Most of them showed increased activity as compared to compound **1**. Especially, compounds **4h** and **4i** completely inhibited the expression of COL1A1 promotor with inhibitory rates of 99.9% at concentrations of 40 and 80 μM . These results indicated that the introduction of a benzene moiety on the 12*N* atom might be beneficial for activity.

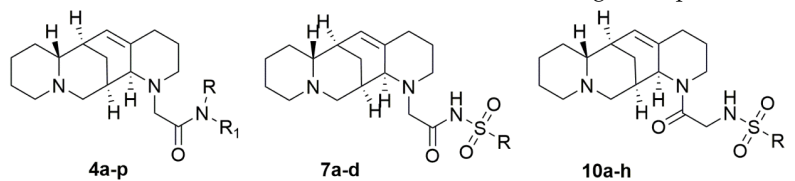
Then, the secondary amine on the carbamoylmethyl linker was transformed into a tertiary amine, and compounds **4m–p** were created. Compounds **4n** and **4p** with bulky substituents displayed higher activity, with inhibitory rates of 99.9% and 72.2% at a concentration of 40 μM , and inhibitory rates of 100.0% and 99.1% at a concentration of 80 μM , respectively. These results indicated again that the introduction of a bulky motif on the 12*N* atom might be helpful for activity.

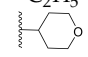
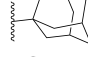
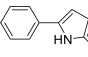
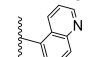
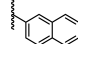
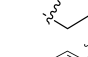

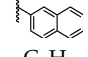
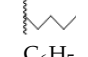
Furthermore, to investigate the possible effect of carbamoylmethyl linker on activity, an additionally sulfonyl group was attached and compounds **7a–d** were generated. The results showed that compounds **7a–d** showed a slight increase in activity. As a comparison, compounds **7a** and **4d**, differing from each other in a sulfonyl group, gave comparable activities, indicating that the insertion of a sulfonyl between the benzene ring and the carbamoylmethyl linker had little effect on potency. At the meantime, an aminoacetyl linker was introduced instead to achieve compounds **10a–g**. The anti-COL1A1 activity results showed that these compounds only gave moderate increases in activity, except **10g**. Notably, compounds **10a** and **10c** gave comparable activity to their counterparts **4a** and **4d**, respectively, while compound **10f** showed decreased activity compared to its counterpart **4g**, indicating that carbamoylmethyl linker on the 12*N* atom might be beneficial.

In the next step, compounds with diverse structural fragments and higher potencies, namely, **4h**, **4i**, **4n**, **4p** and **10g** were selected as representative compounds to examine their acute effects on luciferase activity, and the result showed that they had minimal inhibition on luciferase at the concentration of 80 μM after a 2-h treatment (Figure S1), indicating their direct effects on COL1A1 promotor. Then, their anti-COL1A1 potencies were verified by testing the half maximal inhibition concentration (IC_{50}) values upon COL1A1 expression expression in LX-2 cells. As displayed in Table 1 and Supplementary Figure S2, compounds **4i**, **4n** and **4p** gave the IC_{50} values of 8.4, 13.3 and 16.5 μM , respectively, while compound **4h** failed to give a dose-dependent inhibition within the given concentration range, which was probably due to its high cytotoxicity as shown in Table 2 and Supplementary Figures S3 and S4. Compounds **4i**, **4n**, **4p** and **10g** gave higher median cytotoxic

concentration (CC₅₀) values of 19.5, 17.1, 34.8 and 68.6 μ M in LX-2 cells, and 22.0, 35.2, 43.7 and 113.4 μ M in HepG2 cells, respectively. Then, compounds **4i**, **4n** and **4p** with the lower IC₅₀ values were selected as the key compounds for further studies.

Table 1. Inhibition of COL1A1 Promotor of all the target compounds.



	R	R ₁	Inhibition Percentage ^a 40 μ M(%)	Inhibition Percentage ^a 80 μ M(%)	IC ₅₀ (μ M) ^b
1	/	/	4.7 \pm 3.7	2.6 \pm 5.2	NT ^c
4a	-C ₂ H ₅	H	7.1 \pm 25.6	33.1 \pm 1.6	NT ^c
4b		H	19.0 \pm 3.8	29.8 \pm 10.0	NT ^c
4c		H	23.7 \pm 7.7	39.2 \pm 1.2	NT ^c
4d	C ₆ H ₅	H	18.6 \pm 8.6	28.3 \pm 2.8	NT ^c
4e	<i>p</i> -FC ₆ H ₄	H	21.4 \pm 1.5	26.5 \pm 0.5	NT ^c
4f	<i>m</i> -CH ₃ C ₆ H ₄	H	21.2 \pm 0.4	33.8 \pm 8.0	NT ^c
4g	<i>m</i> -CF ₃ OC ₆ H ₄	H	67.8 \pm 14.9	95.5 \pm 5.5	NT ^c
4h		H	100.0 \pm 0.0	99.9 \pm 0.0	NC ^d
4i	3-Cl-5-CF ₃ OC ₆ H ₃	H	99.9 \pm 0.0	99.9 \pm 0.0	8.4 \pm 0.3
4j	2-CH ₃ -5-CO ₂ CH ₃ C ₆ H ₃	H	3.8 \pm 6.1	32.4 \pm 2.7	NT ^c
4k	3,4,5-tri-CH ₃ C ₆ H ₂	H	50.1 \pm 6.9	70.7 \pm 1.5	NT ^c
4l		H	31.5 \pm 2.6	22.4 \pm 16.1	NT ^c
4m	C ₆ H ₅	CH ₃	19.9 \pm 5.2	34.6 \pm 2.5	NT ^c
4n	C ₆ H ₅		99.9 \pm 0.1	100.0 \pm 0.0	13.3 \pm 0.5
4o			16.5 \pm 9.8	36.7 \pm 9.9	NT ^c
4p			72.2 \pm 1.5	99.1 \pm 1.0	16.5 \pm 0.4
7a	C ₆ H ₅	/	21.5 \pm 4.3	17.1 \pm 6.3	NT ^c
7b	<i>m</i> -CF ₃ C ₆ H ₄	/	23.5 \pm 13.5	20.2 \pm 1.9	NT ^c
7c	3-CF ₃ -4-BrC ₆ H ₃	/	32.9 \pm 3.4	31.8 \pm 3.1	NT ^c
7d		/	18.8 \pm 5.2	9.4 \pm 3.7	NT ^c
10a	C ₂ H ₅	/	34.0 \pm 7.0	34.9 \pm 14.7	NT ^c
10b		/	41.1 \pm 9.6	23.7 \pm 22.7	NT ^c
10c	C ₆ H ₅	/	23.7 \pm 8.3	20.2 \pm 6.4	NT ^c
10d	<i>m</i> -BrC ₆ H ₄	/	28.5 \pm 12.3	27.1 \pm 10.1	NT ^c
10e	<i>m</i> -CF ₃ C ₆ H ₄	/	29.7 \pm 5.1	26.7 \pm 21.3	NT ^c
10f	<i>m</i> -CF ₃ OC ₆ H ₄	/	43.4 \pm 15.9	41.4 \pm 7.4	NT ^c
10g	3,5-di-CF ₃ C ₆ H ₃	/	48.4 \pm 24.7	84.0 \pm 0.5	27.6 \pm 3.0
EGCG	/	/	27.5 \pm 7.9 ^e	NT ^e	NT ^c
DMSO	/	/	2.9 \pm 0	2.9 \pm 0	NT ^c

^a The inhibition rate of COL1A1 promotor's activity at different concentrations in LX-2 cells; ^b Inhibition concentration required to inhibit 50% of COL1A1 promotor's activity in LX-2 cells; ^c Not tested; ^d Not calculatable; ^e At the concentration of 25 μ M

Table 2. The cytotoxicity of representative compounds.

No.	CC ₅₀ (μM) ^a		No.	CC ₅₀ (μM) ^a	
	LX-2	HepG2		LX-2	HepG2
4h	7.5 ± 0.4	18.0 ± 1.9	4p	34.8 ± 2.9	43.7 ± 2.7
4i	19.5 ± 1.8	22.0 ± 4.6	10g	68.6 ± 11.7	113.4 ± 3.4
4n	17.1 ± 5.4	35.2 ± 4.1			

^a Cytotoxic concentration required to inhibit 50% of cell growth of LX-2 or HepG2 cells. The experiment was repeated for 3 times.

2.3. Key Compounds Inhibited the Expression of COL1A1 on mRNA and Protein Levels

In the absence or presence of TGF-β1 (2 ng/mL) treatment, LX-2 cells were treated with key compounds **4n** and **4p** at concentrations of 6 μM and 12 μM, or **4i** at a concentration of 12 μM, respectively.

As shown in Figure 2A and Supplementary Table S1, in the absence of TGF-β1, real-time PCR (RT-PCR) amplification results indicated that the key compounds might lower the transcription of COL1A1, and compound **4n** gave inhibitory rates of 42% and 47% at concentrations of 6 μM and 12 μM, compound **4p** gave inhibitory rates of 38% and 42% at concentrations of 6 μM and 12 μM, and compound **4i** gave an inhibitory rate of 45%, respectively. At the meantime, upon the stimulation of TGF-β1, the transcription of COL1A1 was significantly upregulated up to three times higher than that of the control ($p < 0.01$). As expected, the administration of the three tested compounds repressed the COL1A1 transcription very significantly ($p < 0.01$) and compound **4n** gave inhibitory rates of 76.0% and 84.5% at concentrations of 6 μM and 12 μM, compound **4p** gave inhibitory rates of 99.5% and 102.9% at concentrations of 6 μM and 12 μM, and compound **4i** gave an inhibitory rate of 97.4%, respectively.

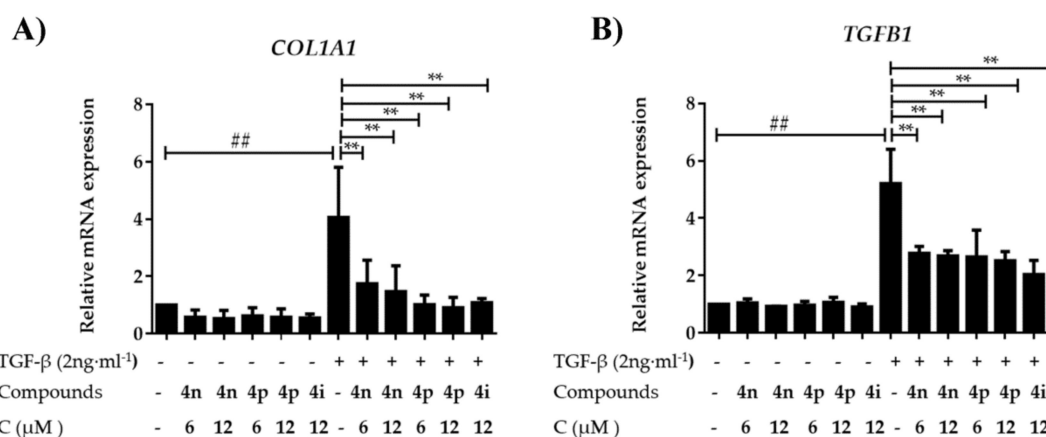


Figure 2. Effects of key compounds (**4i**, **4n** and **4p**) inhibiting COL1A1 (A) and TGFβ1 (B) and on mRNA level in LX-2 cells after a 24 h treatment. Data were analyzed by Real-time PCR, and presented as the mean ± SEM, $p < 0.05$, (##) $p < 0.01$ as compared to that of control group; $p < 0.05$, (**) $p < 0.01$ as compared to that of TGF-β1 group. The mRNA expression levels were normalized against GAPDH. The experiment was repeated three times.

Then the anti-COL1A1 effects of **4n** and **4p** on protein level were evaluated by western blot assay. Without TGF-β1, there was only tiny amounts of COL1A1 expressed in LX2 cells, while the TGF-β1 treatment upregulated the expression of COL1A1 significantly. As displayed in Figure 3A–C and Supplementary Table S2, compound **4n** dose-dependently reversed the increase of COL1A1 protein with the inhibition rates of 31.8% and 76.5%, and compound **4p** gave the dose-dependent inhibition rates of 22.7% and 79.2% at the concentrations of 6 μM and 12 μM, respectively. These results

suggested that these key compounds could effectively reduce COL1A1 expression on both mRNA and protein levels.

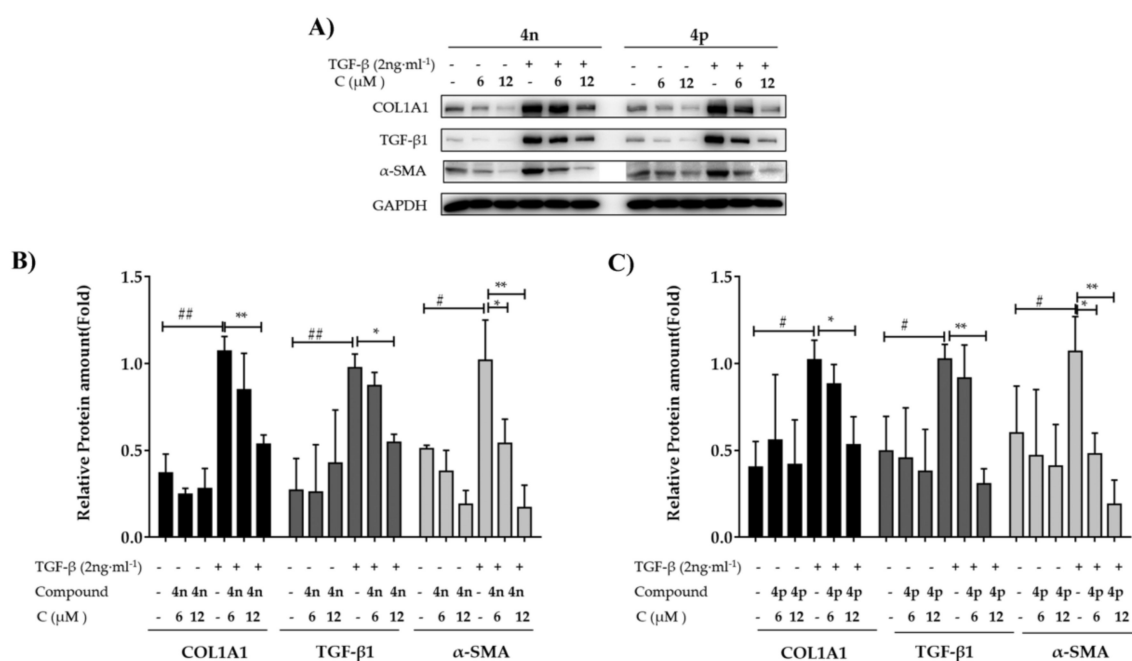


Figure 3. (A) Effects of compounds **4n** and **4p** on inhibiting fibrogenic COL1A1, TGF-β and α-SMA on protein level in LX-2 cells by western blot assay after a 24 h treatment. (B) Gray scanning analysis of **4n** on inhibiting fibrogenic COL1A1, TGF-β and α-SMA on protein level. (C) Gray scanning analysis of **4p** on inhibiting fibrogenic COL1A1, TGF-β and α-SMA on protein level. Data were presented as the mean ± SEM, (#) $p < 0.05$, (##) $p < 0.01$ as compared to that of control group; (*) $p < 0.05$, (**) $p < 0.01$ as compared to that of TGF-β1 group. The protein expression levels were normalized against GAPDH. The experiment was repeated three times.

2.4. Key Compounds Inhibited the Expression of TGF-β on mRNA and Protein Levels

Since the stimulation of TGF-β1 provokes the expression of a series of fibrosis genes, for example COL1A1 and TGFB1 [24,25], the effects of key compounds on TGF-β1 expression were evaluated by RT-PCR and western blot assays. As shown in Figure 2B and Supplementary Table S1, the expression of TGFB1 mRNA was maintained at a low level, and the addition of a key compound seemed to have little effect on its expression. Then, the addition of TGF-β1 caused an abnormally increased expression of TGFB1 itself on mRNA level, which could be reversed significantly by the treatments of **4n**, **4p** or **4i**. Compound **4n** gave inhibitory rates of 57.7% and 60.0% at concentrations of 6 μM and 12 μM, compound **4p** gave inhibitory rates of 60.8% and 63.8% at concentrations of 6 μM and 12 μM, and compound **4i** gave an inhibitory rate of 75.4%, respectively, which showed a good consistency with the above anti-COL1A1 results.

At the meantime, the addition of TGF-β1 also stimulated the expression of TGF-β1 on protein level, as shown in Figure 3A–C and Supplementary Table S2. Both **4n** and **4p** treatment displayed a dose-dependent inhibition on TGF-β1 expression, compound **4n** gave inhibition rates of 14.6% and 61.0%, and compound **4p** gave dose-dependent inhibition rates of 20.8% and 135.4% at concentrations of 6 μM and 12 μM, respectively. Therefore, **4n** and **4p** could inhibit TGF-β1 expression and might block fibrogenesis due to the essential role of TGF-β1 in fibrogenesis [6].

2.5. Key Compounds Inhibited the Expressions of α-SMA on Protein Level

Stellate cell activation is a key process for liver fibrogenesis, and α-SMA expression, induced by a stimulation of TGF-β1 or other factors, is considered a reliable marker of hepatic stellate cell activation

and a key biomarker for liver fibrosis [7,26]. Therefore, the expression of α -SMA was also investigated. As presented in Figure 3A–C and Supplementary Table S2, in our experiments, the addition of TGF- β 1 stimulated the expression of α -SMA on protein level as expected. Similarly, a dose-dependent inhibition of α -SMA expression were observed in both treatments of **4n** and **4p**. These results disclosed that the key compounds might also inhibited the expression of fibrogenic α -SMA.

2.6. Safety Profile of Key Compounds

To evaluate the safety profiles of the key compounds **4i**, **4n** and **4p**, an acute toxicity test was performed in Kunming mice. Compound **4i** was given orally in a single-dosing experiment at 100, 300 and 400 mg kg⁻¹, while **4n** at 300, 400, 500 mg kg⁻¹, and **4p** at 200, 400, 500 mg kg⁻¹. The mice were closely monitored for 7 days. Compound **4n** and **4p** gave their median lethal dose (LD₅₀) values of 500 mg kg⁻¹ and 400 mg kg⁻¹, as shown in Table 3, indicating good safety profiles in vivo.

Table 3. LD₅₀ values of key compounds in vivo.

Compound	LD ₅₀ (mg/kg)
4i	100
4n	500
4p	400

2.7. Discussion

There are few studies on the anti-fibrotic effect of compound **1**, except one by Yin et al. that found that aloperine showed anti-pulmonary fibrosis by attenuating fibroblast proliferation and differentiation via repressed PI3K/AKT/mTOR signaling and TGF- β /Smad signaling [22]. In view of the similar pathogenesis between fibrosis among tissues, our current study elucidated the anti-liver fibrogenesis effect of aloperine and its kind, in the aim of exploring the potential role of aloperine analogues in other types of tissues fibrosis.

Overexpression of collagen is a basic feature of liver fibrosis, and also an important cause of organic lesions [7,11,12]. Taking advantage of this mechanism, Stefanovic et al. [27] established a high-throughput screening model of antifibrotic drugs targeting protein-protein interaction between type I collagen 5'SL and larp6, based on the fact that the COL1A1 5'SL and Arp6 interaction plays an important role in collagen production. In our design to construct a COL1A1-based model, the high expression of COL1A1 in various liver fibrosis processes especially at the transcriptional level was considered. Therefore, the selected compounds by this model inhibited the activity of COL1A1 promoter and thus might hold the advantage of dealing with multi-type tissue fibrosis.

Through systematic structural modification and optimization, aloperine derivatives **4p** was identified to show high potency on inhibiting the COL1A1 promoter and suppressing the expression of fibrogenic proteins COL1A1, TGF- β 1, and α -SMA, with low cytotoxicity and high LD₅₀ values in acute toxicity test, indicating the promise against liver fibrogenesis. The down-regulating COL1A1 mechanism of aloperine derivatives deserves further investigation.

3. Materials and Methods

3.1. Apparatus, Materials, and Analysis Reagents

All solvents and chemical reagents were used as purchased without any further treatment. Aloperine was purchased from the Yanchi Dushun Biological and Chemical Co. Ltd. (Shanxi, China), with the purity over 95%. Room temperature (rt) refers to 20–25 °C. Melting point (mp) was determined on MP90 melting point apparatus and was uncorrected (Mettler-Toledo, Greifensee, Switzerland). ¹H-NMR and ¹³C-NMR spectra were recorded on a Avance 400 MHz or 500 MHz (Bruker, Zürich, Switzerland) and 600 MHz instruments (Bruker, Zürich, Switzerland), taking DMSO-*d*₆ or CDCl₃, as the solvent. ESI high-resolution mass spectrometry (ESI-HRMS) was performed on an AutospecUltima-TOF

mass spectrometer (Micromass UK Ltd., Manchester, UK). Flash chromatography was performed on a Combiflash Rf 200 system (Teledyne, Lincoln, NE, USA).

3.2. Chemistry

3.2.1. General Procedure for 12N-Substituted Carbamoylmethyl Aloperine Derivatives (4a–p)

To a solution of substituted amine **2a–p** (2 mmol) in anhydrous dichloromethane (30 mL), triethylamine (0.3 mL, 2 mmol) was added and stirred at 0 °C, and then bromoacetyl bromide (0.4 g, 2 mmol) was slowly added. After 30 min, the reaction system was warmed to room temperature, stirred for 1.5 h, then triethylamine (0.3 mL, 2 mmol) and **1** (0.5 g, 2 mmol) were added and stirred overnight at room temperature until the TLC analysis showed completion of the reaction. The resulting mixture was washed with water and brine, dried over anhydrous Na₂SO₄, filtered and concentrated to give a residue, which was purified by flash column chromatography on silica gel with dichloromethane/methanol as the eluent to furnish the title compounds.

12N-N'-Ethylcarbamoylmethyl aloperine (4a), Yield 38%; brown solid; m.p.: 69–71 °C. ¹H-NMR (400 MHz, CDCl₃) δ 9.16 (s, 1H), 9.01 (s, 1H), 5.85 (d, *J* = 5.2 Hz, 1H), 4.60–4.40 (m, 2H), 4.32–4.16 (m, 1H), 4.15–4.04 (m, 1H), 3.99–3.72 (m, 3H), 3.61–3.44 (m, 2H), 3.42–3.32 (m, 1H), 3.29–3.16 (m, 3H), 2.98–2.81 (m, 1H), 2.60–2.49 (m, 1H), 2.43–2.34 (m, 1H), 2.32–2.21 (m, 2H), 2.18–2.06 (m, 1H), 2.01–1.85 (m, 2H), 1.83–1.64 (m, 4H), 1.56–1.42 (m, 1H), 1.20 (s, 1H), 1.14 (t, *J* = 7.2 Hz, 3H). ¹³C-NMR (101 MHz, CDCl₃) δ 163.4, 135.7, 127.7, 63.5, 59.3, 56.0, 55.1, 53.3, 46.2, 34.7, 33.6, 30.7, 27.7, 24.2, 23.5, 22.6, 21.2, 18.4, 14.3. ESI-HR-MS: calcd. for: C₁₉H₃₂N₃O [M + H]⁺, 318.2540, found: 318.2530.

12N-N'-(Tetrahydro-2H-pyran-4-yl)carbamoylmethyl aloperine hydrochloride (4b), Yield 29%; white solid; m.p.: 199–201 °C. ¹H-NMR (400 MHz, CDCl₃) δ 11.16 (s, 1H), 9.52 (d, *J* = 5.2 Hz, 1H), 9.16 (s, 1H), 5.88 (d, *J* = 5.2 Hz, 1H), 4.71–4.58 (m, 1H), 4.44 (s, 1H), 4.11–4.04 (m, 1H), 4.01–3.91 (m, 4H), 3.90–3.83 (m, 2H), 3.76 (s, 1H), 3.68–3.53 (m, 2H), 3.48–3.38 (m, 2H), 3.36–3.27 (m, 2H), 3.22–3.10 (m, 1H), 3.09–2.95 (m, 1H), 2.63–2.52 (m, 1H), 2.41 (s, 1H), 2.36–2.21 (m, 2H), 2.19–2.06 (m, 1H), 2.04–1.97 (m, 1H), 1.91–1.80 (m, 3H), 1.80–1.68 (m, 4H), 1.56–1.43 (m, 1H). ¹³C-NMR (101 MHz, CDCl₃) δ 162.9, 135.9, 127.6, 66.5 (2), 63.6, 59.5, 56.4, 55.2, 53.4, 46.5, 46.4, 33.6, 32.2, 32.2, 30.8, 27.8, 24.3, 23.6, 22.6, 21.1, 18.5. ESI-HR-MS: calcd. for: C₂₂H₃₆N₃O₂ [M + HCl-Cl]⁺, 374.2802, found: 374.2795.

12N-N'-Adamantylcarbamoylmethyl aloperine (4c), Yield 17%; brown solid; m.p.: 176–178 °C. ¹H-NMR (400 MHz, CDCl₃) δ 7.31 (s, 1H), 5.67 (s, 1H), 3.87–3.73 (m, 1H), 3.44–3.32 (m, 1H), 3.26–3.12 (m, 2H), 3.11–2.95 (m, 3H), 2.95–2.82 (m, 2H), 2.59–2.43 (m, 3H), 2.31–2.15 (m, 3H), 2.10–2.03 (m, 8H), 1.96–1.89 (m, 5H), 1.70–1.61 (m, 9H), 1.56–1.48 (m, 2H). ¹³C-NMR (101 MHz, CDCl₃) δ 169.4, 140.3, 122.3, 63.1, 61.8, 58.1, 57.1, 56.0, 54.2, 52.2, 51.2, 45.5, 41.9 (3), 36.4 (3), 33.8, 33.1, 29.5 (3), 25.7, 23.8, 22.8, 18.8. ESI-HR-MS: calcd. for: C₂₇H₄₂N₃O [M + H]⁺, 424.3322, found: 424.3311.

12N-N'-Phenylcarbamoylmethyl aloperine (4d), Yield 55%; white solid; m.p.: 66–68 °C. ¹H-NMR (400 MHz, CDCl₃) δ 7.19 (t, *J* = 7.6 Hz, 2H), 6.71 (t, *J* = 7.2 Hz, 1H), 6.63 (d, *J* = 8.0 Hz, 2H), 5.64 (d, *J* = 4.0 Hz, 1H), 4.95 (s, 1H), 4.75 (d, *J* = 4.0 Hz, 1H), 4.01–3.93 (m, 1H), 3.88–3.80 (m, 1H), 3.79–3.67 (m, 1H), 3.47–3.39 (m, 1H), 3.09–3.01 (m, 1H), 2.74 (d, *J* = 8.0 Hz, 2H), 2.63–2.55 (m, 1H), 2.44 (s, 1H), 2.39–2.31 (m, 1H), 2.31–2.21 (m, 1H), 2.17–2.06 (m, 1H), 1.97 (s, 1H), 1.94–1.83 (m, 4H), 1.83–1.76 (m, 1H), 1.69 (m, 2H), 1.51–1.39 (m, 1H), 1.15–1.02 (m, 2H). ¹³C-NMR (101 MHz, CDCl₃) δ 167.8, 147.6, 135.4, 129.4 (2), 128.4, 117.5, 113.1 (2), 59.4, 59.2, 54.4, 46.9, 45.5, 40.6, 35.1, 31.5, 28.0, 26.3, 24.9, 24.6, 24.1, 19.2. ESI-HR-MS: calcd. for: C₂₃H₃₂N₃O [M + H]⁺: 366.2540, found: 366.2541.

12N-N'-(4-Fluorophenyl)carbamoylmethyl aloperine (4e), Yield 50%; white solid; mp 119–121 °C. ¹H-NMR (500 MHz, CDCl₃) δ 9.25 (s, 1H), 7.57–7.43 (m, 2H), 7.01 (t, *J* = 8.5 Hz, 2H), 5.62 (d, *J* = 5.0 Hz, 1H), 3.68–3.52 (m, 1H), 2.92 (d, *J* = 5.0 Hz, 2H), 2.80–2.71 (m, 1H), 2.70–2.62 (m, 2H), 2.60–2.52 (m, 1H), 2.48–2.42 (m, 1H), 2.34–2.24 (m, 2H), 2.22–2.14 (m, 1H), 2.08–1.97 (m, 2H), 1.93–1.84 (m, 2H), 1.80–1.66 (m, 2H), 1.64–1.50 (m, 2H), 1.50–1.42 (m, 2H), 1.42–1.35 (m, 1H), 1.34–1.23 (m, 2H); ¹³C-NMR (126 MHz, CDCl₃) δ 169.5, 159.4, 134.1, 133.0, 129.3, 121.0, 121.0, 116.0,

115.8, 64.3, 63.9, 57.3, 55.9, 55.3, 51.7, 35.8, 33.4, 31.6, 30.3, 26.2, 25.5, 24.8, 23.8. ESI-HR-MS: calcd. for: $C_{23}H_{31}FN_3O$ $[M + H]^+$: 384.2446, found: 384.2443.

12N-N'-(3-Methylphenyl)carbamoylmethyl aloperine (4f), Yield 51%; white solid; mp 40–42 °C. 1H -NMR (500 MHz, $CDCl_3$) δ 9.19 (s, 1H), 7.39 (s, 1H), 7.32 (d, $J = 7.5$ Hz, 1H), 7.21 (t, $J = 8.0$ Hz, 1H), 6.91 (d, $J = 7.0$ Hz, 1H), 5.64 (s, 1H), 3.65–3.56 (m, 1H), 3.09 (s, 1H), 2.92 (s, 2H), 2.79–2.65 (m, 2H), 2.59 (s, 1H), 2.52–2.45 (m, 1H), 2.34 (s, 3H), 2.31–2.15 (m, 2H), 2.09–1.99 (m, 2H), 1.92 (s, 2H), 1.81–1.73 (m, 1H), 1.72–1.66 (m, 1H), 1.65–1.54 (m, 2H), 1.52–1.44 (m, 2H), 1.44–1.36 (m, 1H), 1.36–1.22 (m, 2H), 0.90–0.81 (m, 1H); ^{13}C -NMR (126 MHz, $CDCl_3$) δ 169.2, 139.0, 137.7, 132.9, 129.0, 128.9, 124.9, 119.8, 116.3, 63.6, 57.2, 55.6, 55.0, 51.4, 35.5, 33.2, 31.4, 30.0, 26.9, 25.9, 25.2, 24.6, 23.5, 21.5. ESI-HR-MS: calcd. for: $C_{24}H_{34}N_3O$ $[M + H]^+$: 380.26964, found: 380.2687.

*12N-N'-(*m*-Trifluoromethoxyphenyl)carbamoylmethyl aloperine (4g)*, Yield 40%; light brown solid; mp 50–52 °C. 1H -NMR (500 MHz, $CDCl_3$) δ 10.16 (s, 1H), 8.30 (s, 1H), 8.11 (d, $J = 7.5$ Hz, 1H), 7.31 (m, 1H), 6.93 (d, $J = 7.5$ Hz, 1H), 5.68 (d, $J = 5.5$ Hz, 1H), 3.65–3.52 (m, 1H), 3.52–3.42 (m, 1H), 3.38–3.30 (m, 1H), 3.30–3.22 (m, 1H), 3.20–3.05 (m, 5H), 2.86–2.75 (m, 1H), 2.61–2.49 (m, 2H), 2.38–2.27 (m, 2H), 2.13–1.89 (m, 4H), 1.80–1.59 (m, 4H), 1.58–1.41 (m, 2H); ^{13}C -NMR (126 MHz, $CDCl_3$) δ 169.5, 149.2, 140.9, 139.9, 129.9, 121.8, 119.3, 116.1, 113.1, 61.7, 58.7, 56.8, 56.5, 56.4, 53.5, 45.5, 33.8, 33.7, 29.4, 24.2, 23.4, 23.0, 22.6, 18.7. ESI-HR-MS: calcd. for: $C_{24}H_{31}F_3N_3O_2$ $[M + H]^+$: 450.2363, found: 450.2351.

*12N-N'-[4-(1*H*-Indol-2-yl)phenyl]carbamoylmethyl aloperine (4h)*, Yield 18%; brown solid; m.p.: 219–221 °C. 1H -NMR (500 MHz, $CDCl_3$) δ 9.77 (s, 1H), 9.32 (s, 1H), 8.20 (d, $J = 7.5$ Hz, 2H), 7.72–7.57 (m, 3H), 7.53–7.46 (m, 1H), 7.19–7.14 (m, 1H), 7.13–7.07 (m, 1H), 6.73 (s, 1H), 5.62 (s, 1H), 3.60 (s, 1H), 3.45–3.31 (m, 1H), 3.27–3.06 (m, 3H), 3.02–2.85 (m, 4H), 2.83–2.72 (m, 1H), 2.58–2.40 (m, 1H), 2.36–2.20 (m, 3H), 2.03–1.77 (m, 4H), 1.68–1.48 (m, 5H), 1.40–1.24 (m, 1H). ^{13}C -NMR (126 MHz, $CDCl_3$) δ 169.0, 140.5, 138.0, 137.4, 136.8, 129.1, 128.0, 125.6 (2), 122.0, 121.7, 120.9, 120.1, 119.9, 111.1, 98.7, 61.6, 58.2, 56.7, 56.5, 56.3, 53.3, 45.3, 33.6, 33.3, 29.1, 23.8, 23.3, 22.6, 22.1, 18.4. ESI-HR-MS: calcd for $C_{31}H_{37}N_4O$ $[M + H]^+$, 481.2962, Found: 481.2964.

12N-N'-(3-Chloro-5-trifluoromethoxyphenyl)carbamoylmethyl aloperine (4i), Yield 35%; light pink solid; m.p.: 44–46 °C. 1H -NMR (400 MHz, $CDCl_3$) δ 9.53 (s, 1H), 7.55 (s, 1H), 7.47 (s, 1H), 6.96 (s, 1H), 5.63 (d, $J = 5.2$ Hz, 1H), 3.63–3.55 (m, 1H), 2.97–2.84 (m, 2H), 2.81–2.73 (m, 1H), 2.72–2.60 (m, 2H), 2.54–2.46 (m, 1H), 2.46–2.38 (m, 1H), 2.36–2.21 (m, 3H), 2.10–1.95 (m, 3H), 1.93 (s, 1H), 1.81–1.74 (m, 1H), 1.72–1.60 (m, 2H), 1.59–1.49 (m, 2H), 1.45–1.28 (m, 4H). ^{13}C -NMR (101 MHz, $CDCl_3$) δ 170.0, 149.9, 140.0, 135.5, 133.3, 129.0, 120.4, 117.5, 116.6, 110.2, 63.7, 63.3, 57.2, 55.7, 55.4, 51.0, 35.6, 33.3, 30.6, 30.4, 25.9, 25.4, 24.0, 23.9. ESI-HR-MS: calcd. for: $C_{24}H_{30}ClF_3N_3O_2$ $[M + H]^+$, 484.1973, found: 484.1965.

12N-N'-(2-Methyl-5-methoxycarbonylphenyl)carbamoylmethyl aloperine (4j), Yield 16%; violet solid; m.p.: 75–77 °C. 1H -NMR (500 MHz, $CDCl_3$) δ 9.46 (s, 1H), 8.51–8.41 (m, 1H), 7.99–7.83 (m, 2H), 5.72–5.61 (m, 1H), 3.90 (s, 3H), 3.77–3.67 (m, 1H), 3.03–2.90 (m, 2H), 2.84–2.72 (m, 1H), 2.65 (s, 2H), 2.49 (s, 1H), 2.39–2.13 (m, 6H), 2.11–1.99 (m, 3H), 1.92 (s, 1H), 1.86–1.67 (m, 3H), 1.61–1.38 (m, 5H), 1.36–1.22 (m, 2H). ^{13}C -NMR (126 MHz, $CDCl_3$) δ 169.7, 167.0, 140.6, 132.6, 131.9, 129.6, 129.1, 125.5, 125.2, 119.2, 64.9, 63.8, 57.7, 56.0, 55.2, 52.2, 52.1, 35.7, 33.4, 32.0, 30.1, 26.1, 25.4, 25.0, 23.7, 18.2. ESI-HR-MS: calcd for $C_{26}H_{36}N_3O_3$ $[M + H]^+$, 438.2751, Found: 438.2752.

12N-N'-(3,4,5-Trimethylphenyl)carbamoylmethyl aloperine (4k), Yield 42%; white solid; m.p.: 183–185 °C. 1H -NMR (400 MHz, $CDCl_3$) δ 7.70 (s, 2H), 5.74 (s, 1H), 3.69–3.48 (m, 3H), 3.38–3.30 (m, 3H), 3.15–3.02 (m, 2H), 2.60–2.52 (m, 1H), 2.32 (s, 1H), 2.26 (s, 8H), 2.12–2.04 (m, 6H), 1.98–1.88 (m, 2H), 1.75–1.66 (m, 4H), 1.65–1.57 (m, 2H), 1.54–1.44 (m, 1H), 1.24 (s, 1H). ^{13}C -NMR (101 MHz, $CDCl_3$) δ 167.5, 139.7, 137.2, 136.9, 135.3, 131.2, 123.2, 119.5, 119.2, 62.1, 58.6, 56.4, 56.2, 56.0, 45.7, 33.8, 33.1, 29.1, 24.1, 23.1, 22.6, 20.8 (3), 18.6, 15.0. ESI-HR-MS: calcd. for: $C_{26}H_{38}N_3O$ $[M + H]^+$, 408.3009, found: 408.2999.

12N-N'-(5-Quinoly)carbamoylmethyl aloperine (4l), Yield 29%; yellow solid; m.p.: 74–76 °C. 1H -NMR (400 MHz, $CDCl_3$) δ 9.94 (s, 1H), 8.95 (d, $J = 3.2$ Hz, 1H), 8.34 (d, $J = 7.2$ Hz, 1H), 8.22 (d, $J = 8.8$ Hz, 1H), 7.92 (d, $J = 8.4$ Hz, 1H), 7.73 (t, $J = 8.0$ Hz, 1H), 7.46 (dd, $J = 8.4, 4.0$ Hz, 1H), 5.69 (d, $J = 4.8$ Hz, 1H), 3.86–3.75 (m, 1H), 3.12–3.04 (m, 1H), 3.00 (s, 1H), 2.93–2.84 (m, 1H), 2.83–2.74 (m, 1H), 2.72–2.52

(m, 3H), 2.43–2.29 (m, 2H), 2.17–2.01 (m, 3H), 1.99–1.86 (m, 2H), 1.82–1.71 (m, 2H), 1.70–1.60 (m, 1H), 1.57–1.45 (m, 2H), 1.44–1.22 (m, 4H). $^{13}\text{C-NMR}$ (101 MHz, CDCl_3) δ 169.7, 150.4, 148.8, 132.9, 132.7, 129.9, 129.4, 128.9, 126.2, 121.0, 120.9, 118.3, 64.3, 63.8, 57.6, 56.0, 55.3, 51.9, 35.7, 33.4, 31.3, 30.3, 26.2, 25.4, 24.5, 23.8. ESI-HR-MS: calcd. for: $\text{C}_{26}\text{H}_{33}\text{N}_4\text{O}$ $[\text{M} + \text{H}]^+$, 417.2649, found: 417.2638.

12N-[(*N'*-Methyl-*N'*-phenyl)carbamoylmethyl aloperine (**4m**), Yield 55%; white solid; m.p.: 73–75 °C. $^1\text{H-NMR}$ (400 MHz, CDCl_3) δ 7.22 (t, $J = 7.6$ Hz, 2H), 6.77–6.67 (m, 3H), 5.61 (d, $J = 4.8$ Hz, 1H), 4.71 (d, $J = 3.2$ Hz, 1H), 4.14–4.08 (m, 1H), 3.69 (s, 1H), 3.55–3.43 (m, 1H), 3.10–2.98 (m, 4H), 2.81–2.69 (m, 2H), 2.62–2.52 (m, 1H), 2.44–2.33 (m, 2H), 2.28–2.19 (m, 1H), 2.16–2.04 (m, 1H), 1.98–1.78 (m, 5H), 1.75–1.59 (m, 4H), 1.46–1.38 (m, 1H), 1.15–1.01 (m, 2H). $^{13}\text{C-NMR}$ (101 MHz, CDCl_3) δ 168.8, 149.6, 135.8, 129.3 (2), 128.1, 117.3, 112.7, 112.4, 59.5, 59.1, 55.0, 54.4, 46.9, 41.2, 39.7, 35.1, 31.4, 28.1, 26.3, 25.0, 24.9, 24.2, 19.3. ESI-HR-MS: calcd. for: $\text{C}_{24}\text{H}_{34}\text{N}_3\text{O}$ $[\text{M} + \text{H}]^+$: 380.2696, found: 380.2696.

12N-(*N'*-(Naphthalen-2-yl)-*N'*-phenyl)carbamoylmethyl aloperine (**4n**), Yield 46%; white solid; m.p.: 79–81 °C. $^1\text{H-NMR}$ (400 MHz, CDCl_3) δ 7.89–7.74 (m, 3H), 7.69 (s, 1H), 7.48 (s, 2H), 7.42–7.34 (m, 3H), 7.33–7.28 (m, 3H), 5.48 (d, $J = 5.6$ Hz, 1H), 3.51–3.41 (m, 1H), 3.41–3.25 (m, 2H), 2.90 (d, $J = 4.4$ Hz, 2H), 2.54 (s, 1H), 2.32–2.15 (m, 3H), 2.07–1.92 (m, 3H), 1.82 (s, 1H), 1.76–1.67 (m, 2H), 1.66–1.59 (m, 2H), 1.55–1.46 (m, 3H), 1.41 (s, 1H), 1.30–1.20 (m, 3H). $^{13}\text{C-NMR}$ (151 MHz, $\text{DMSO-}d_6$) δ 163.7, 141.7, 139.3, 137.7, 134.4, 133.2, 130.3, 129.0, 128.6, 128.2, 127.7, 127.6, 127.4, 127.2, 127.0, 126.8, 126.0, 125.2, 124.9, 63.4, 58.1, 55.0, 53.8, 53.0, 44.6, 32.5, 30.1, 27.0, 22.9, 22.6, 21.9, 20.3, 17.7. ESI-HR-MS: calcd. for: $\text{C}_{33}\text{H}_{38}\text{N}_3\text{O}$ $[\text{M} + \text{H}]^+$, 492.3009, found: 492.2994.

12N-*N'*-(1-Pyrrolidinyl)carbamoylmethyl aloperine (**4o**), Yield 50%; brown solid; m.p.: 78–80 °C. $^1\text{H-NMR}$ (400 MHz, CDCl_3) δ 9.61 (s, 1H), 6.02–5.78 (m, 1H), 5.74–5.48 (m, 2H), 5.07–4.85 (m, 1H), 4.67–4.54 (m, 1H), 4.48–4.32 (m, 1H), 3.99–3.84 (m, 1H), 3.79–3.71 (m, 1H), 3.69–3.59 (m, 2H), 3.56–3.37 (m, 4H), 3.37–3.25 (m, 2H), 3.21–2.84 (m, 2H), 2.62–2.48 (m, 1H), 2.40–2.28 (m, 2H), 2.27–2.12 (m, 1H), 2.09–1.88 (m, 4H), 1.87–1.79 (m, 3H), 1.78–1.56 (m, 3H), 1.54–1.40 (m, 1H). $^{13}\text{C-NMR}$ (101 MHz, CDCl_3) δ 161.9, 136.1, 127.4, 64.0, 59.5, 56.4, 55.2, 53.8, 46.5, 46.5, 46.0, 33.6, 30.8, 27.5, 26.1, 24.3, 24.1, 23.5, 22.7, 21.0, 18.4. ESI-HR-MS: calcd. for: $\text{C}_{21}\text{H}_{34}\text{N}_3\text{O}$ $[\text{M} + \text{H}]^+$: 344.2696, found: 344.2683.

12N-*N'*-Phenoxazinylcarbamoylmethyl aloperine (**4p**), Yield 56%; light brown solid; m.p.: 84–86 °C. $^1\text{H-NMR}$ (400 MHz, CDCl_3) δ 7.50–7.44 (m, 2H), 7.22–7.16 (m, 2H), 7.15–7.08 (m, 4H), 5.48 (d, $J = 5.2$ Hz, 1H), 3.79–3.60 (m, 2H), 3.34 (s, 1H), 2.92–2.68 (m, 3H), 2.52–2.38 (m, 3H), 2.20–2.13 (m, 1H), 2.11–1.91 (m, 3H), 1.83 (s, 1H), 1.78–1.68 (m, 2H), 1.61–1.51 (m, 3H), 1.48–1.38 (m, 3H), 1.32–1.20 (m, 2H). $^{13}\text{C-NMR}$ (101 MHz, CDCl_3) δ 169.4, 151.3 (2), 133.5, 129.1 (2), 127.6 (2), 127.2, 125.2 (2), 123.6 (2), 117.3 (2), 66.1, 62.1, 55.9, 54.2, 52.9, 51.8, 35.6, 33.3, 32.9, 29.5, 26.3, 25.6, 25.1, 23.4. ESI-HR-MS: calcd. for: $\text{C}_{29}\text{H}_{34}\text{N}_3\text{O}_2$ $[\text{M} + \text{H}]^+$, 456.2646, found: 456.2638.

3.2.2. General Procedures for 12N-Substituted Sulfonylcarbamoylmethyl Aloperine Derivatives (**7a–d**)

To a solution of substituted sulfanilamide (2 mmol) in toluene (20 mL), bromoacetyl bromide (0.8 g, 4 mmol) was added dropwise, the mixture was stirred at 0 °C for 30 min, then reaction was stirred at 90 °C for 5 h. The reaction was monitored by TLC until TLC showed the completion of the reaction. Then the mixture was evaporated, and the gained residue was suspended in saturated NaHCO_3 solution (40 mL). The mixture was filtered, and conc. HCl solution was added dropwise to the filtrate to precipitate the intermediates **6a–d**, which was applied to the next step without further purification. To a solution of **6a–d** (1 mmol) in DMF (30 mL), **1** (1.2 mmol) and K_2CO_3 (3 mmol) was added. The mixture was heated at 100 °C and stirred overnight. The mixture was evaporated, and the residue was dissolved in dichloromethane, filtered and purified by flash column chromatography on silica gel with dichloromethane/methanol as the eluent to give the title compounds **7a–d**.

12N-*N'*-Benzenesulfonyl carbamoylmethyl aloperine (**7a**), Yield: 40%; light yellow solid, m.p.: 113–115 °C. $^1\text{H-NMR}$ (400 MHz, CDCl_3) δ 7.99 (dd, $J = 8.0, 1.6$ Hz, 2H), 7.47–7.35 (m, 3H), 5.66 (d, $J = 6.0$ Hz, 1H), 3.55–3.45 (m, 1H), 3.36 (d, $J = 4.8$ Hz, 1H), 3.25–2.90 (m, 7H), 2.74–2.61 (m, 1H), 2.54 (s, 1H), 2.34–2.23 (m, 1H), 2.14–2.09 (m, 1H), 2.08–1.96 (m, 2H), 1.93–1.82 (m, 2H), 1.81–1.60 (m, 3H), 1.57–1.41 (m, 4H), 1.29–1.23 (m, 1H). $^{13}\text{C-NMR}$ (101 MHz, CDCl_3) δ 174.0, 144.3 137.6, 131.0,

128.2(2), 127.1(2), 125.8, 62.7, 59.5, 55.2, 54.6, 46.8, 34.1, 33.1, 31.7, 29.1, 24.9, 23.5, 22.7, 22.7, 19.6. ESI-HR-MS: calcd for $C_{23}H_{32}N_3O_3S$ [M + H]⁺: 430.2159, found: 430.2147.

12N-N'-3-Trifluoromethylbenzenesulfonyl carbamoylmethyl aloperine (**7b**). Yield: 22%; light yellow solid, m.p.: 105–107 °C. ¹H-NMR (400 MHz, CDCl₃) δ 8.23–8.14 (m, 2H), 7.65 (d, *J* = 7.6 Hz, 1H), 7.52 (t, *J* = 7.6 Hz, 1H), 5.59 (d, *J* = 6.0 Hz, 1H), 3.45–3.36 (m, 1H), 3.34–3.14 (m, 7H), 2.97–2.88 (m, 1H), 2.56–2.40 (m, 2H), 2.30–2.22 (m, 1H), 2.16 (s, 1H), 2.05–1.84 (m, 5H), 1.83–1.75 (m, 1H), 1.66–1.46 (m, 5H). ¹³C-NMR (101 MHz, CDCl₃) δ 175.2, 146.0, 138.6, 130.7, 130.4, 128.7, 127.3, 125.1, 124.2, 123.9, 62.6(2), 60.1, 55.3, 54.5, 46.1, 34.0, 33.3, 29.2, 24.9, 24.1, 23.4, 23.2, 19.1. ESI-HR-MS: calcd for $C_{24}H_{31}F_3N_3O_3S$ [M + H]⁺: 498.2033, found: 498.2019.

12N-N'-(4-Bromo-3-trifluoromethylbenzenesulfonyl)carbamoylmethyl aloperine (**7c**). Yield: 12%; white solid, m.p.: 79–81 °C. ¹H-NMR (600 MHz, CDCl₃) δ 8.25 (s, 1H), 8.07 (d, *J* = 7.8 Hz, 1H), 7.74 (d, *J* = 7.8 Hz, 1H), 5.67 (d, *J* = 4.8 Hz, 1H), 3.49–3.16 (m, 6H), 3.15–3.06 (m, 1H), 3.02–2.90 (m, 1H), 2.61–2.39 (m, 2H), 2.37–2.27 (m, 1H), 2.21 (s, 1H), 2.07–1.83 (m, 5H), 1.64–1.47 (m, 5H), 1.30–1.19 (m, 3H). ¹³C-NMR (101 MHz, CDCl₃) δ 173.4, 144.6, 140.2, 134.8, 132.0, 129.8, 127.0, 123.7, 122.8, 122.6, 62.4, 60.2, 59.0, 55.2, 54.5, 46.1, 33.9, 33.4, 29.2, 24.4, 23.1, 23.0, 22.8, 18.7. ESI-HR-MS: calcd for $C_{25}H_{30}BrF_3N_3O_3S$ [M + H]⁺: 576.1138, found: 576.1122.

12N-N'-(1-Naphtylsulfonyl)carbamoylmethyl aloperine (**7d**). Yield: 31%; white solid, m.p.: 93–95 °C. ¹H-NMR (600 MHz, CDCl₃) δ 8.70 (s, 1H), 8.12 (dd, *J* = 8.4, 1.6 Hz, 1H), 8.02 (d, *J* = 7.8 Hz, 1H), 7.97 (d, *J* = 8.4 Hz, 1H), 7.90 (d, *J* = 8.4 Hz, 1H), 7.64 (t, *J* = 7.2 Hz, 1H), 7.60 (t, *J* = 7.2 Hz, 1H), 5.70 (d, *J* = 6.0 Hz, 1H), 3.89–3.77 (m, 1H), 3.52 (s, 1H), 3.48–3.36 (m, 3H), 3.36–3.26 (m, 3H), 3.00–2.92 (m, 1H), 2.75–2.63 (m, 2H), 2.42–2.35 (m, 1H), 2.31 (s, 1H), 2.13–2.00 (m, 4H), 2.00–1.91 (m, 2H), 1.75–1.65 (m, 3H), 1.65–1.60 (m, 1H), 1.58–1.47 (m, 2H). ¹³C-NMR (101 MHz, CDCl₃) δ 173.3, 141.5, 138.7, 134.3, 132.4, 129.3, 128.1, 127.7, 127.7, 127.6, 126.7, 124.8, 123.8, 62.6 (2), 59.9, 55.3, 54.4, 46.4, 34.0, 33.2, 29.1, 24.6, 23.4, 23.3, 22.7, 19.1. ESI-HR-MS: calcd for $C_{27}H_{34}N_3O_3S$ [M + H]⁺: 480.2315, found: 480.2311.

3.2.3. General Procedures for 12N-sulfonylaminoacetylaloperine Derivatives **10a–g**

To a solution of glycine (3 mmol) and NaOH (3.6 mL) in H₂O (15 mL), the substituted sulphonyl chloride **8a–g** (3.3 mmol) was slowly added at 0 °C, then the mixture was stirred at room temperature for 3 h. After the mixture was adjusted to pH 2 by 20% aqueous hydrochloric acid, brine (30 mL) was added, and the gained mixture was extracted with dichloromethane (30 mL × 2). The organic layer was dried over anhydrous Na₂SO₄ and concentrated under vacuum to afford intermediates **9a–g** without further purification.

To the solution of **9a–g** in dichloromethane (30 mL) at 0 °C, N-hydroxybenzotriazol (HOBT, 4 mmol), 1-ethyl-3-(3-dimethylaminopropyl) carbodiimide (EDCI, 6 mmol) and diisopropyl-ethylamine (1.3 mL) was added and stirred for 30 min, followed by addition of **1** (3 mmol). The reaction was warmed to room temperature, stirred for 12 h. The mixture was washed with water (50 mL × 2) and brine (50 mL), dried over anhydrous Na₂SO₄, filtered and then the filtrate was concentrated in vacuum. Then the residue was purified by flash column chromatography on silica gel with dichloromethane/methanol as the eluent to give target compounds **10a–g**.

12N-N'-Ethylsulfonylaminoacetyl aloperine (**10a**). Yield: 51%; white solid; mp 145–147 °C. ¹H-NMR (400 MHz, CDCl₃) δ 5.67–5.60 (m, 1H), 5.38–5.31 (m, 1H), 4.68 (d, *J* = 4.8 Hz, 1H), 4.07–3.99 (m, 1H), 3.93–3.84 (m, 1H), 3.77–3.65 (m, 1H), 3.31–3.21 (m, 1H), 3.13–2.99 (m, 3H), 2.73 (d, *J* = 7.4 Hz, 2H), 2.62–2.53 (m, 1H), 2.41–2.22 (m, 2H), 2.15–2.03 (m, 1H), 2.02–1.94 (m, 1H), 1.91–1.59 (m, 8H), 1.50–1.35 (m, 4H), 1.15–1.00 (m, 2H). ¹³C-NMR (101 MHz, CDCl₃) δ 166.2, 134.9, 128.7, 59.4, 59.3, 54.4, 47.4, 46.7, 44.4, 40.8, 34.9, 31.4, 27.8, 26.1, 24.7, 24.5, 24.0, 19.2, 8.4. ESI-HR-MS: calcd for $C_{19}H_{32}N_3O_3S$ [M + H]⁺: 382.2159, found: 382.2151.

12N-N'-*n*-Butylsulfonylaminoacetyl aloperine (**10b**). Yield: 47%; white solid; m.p.: 98–100 °C. ¹H-NMR (400 MHz, CDCl₃) δ 9.90 (s, 1H), 5.80 (s, 1H), 4.76 (s, 1H), 4.22–3.98 (m, 2H), 3.94–3.78 (m, 2H), 3.63–3.26 (m, 3H), 3.21–2.96 (m, 4H), 2.84 (s, 1H), 2.75–2.57 (m, 1H), 2.33 (s, 1H), 2.29–2.12 (m, 2H), 2.10–2.02 (m, 1H), 2.01–1.89 (m, 2H), 1.86–1.66 (m, 7H), 1.61–1.51 (m, 1H), 1.50–1.39 (m, 2H), 1.27–1.21

(m, 1H), 0.94 (t, $J = 7.2$ Hz, 3H). $^{13}\text{C-NMR}$ (101 MHz, CDCl_3) δ 167.9, 137.5, 126.1, 58.2, 58.1, 54.8, 53.1, 45.6, 44.7, 43.0, 33.9, 29.5, 27.2, 25.6, 24.0, 22.8, 22.5, 22.2, 21.6, 18.8, 13.7. ESI-HR-MS: calcd for $\text{C}_{21}\text{H}_{36}\text{N}_3\text{O}_3\text{S} [\text{M} + \text{H}]^+$: 410.2472, found: 410.2461.

12N-N'-Benzenesulfonylaminoacetylaloperine (10c), Yield: 45%; white solid; m.p.: 63–65 °C. $^1\text{H-NMR}$ (400 MHz, CDCl_3) δ 7.88 (d, $J = 7.2$ Hz, 2H), 7.58 (t, $J = 7.2$ Hz, 1H), 7.51 (t, $J = 7.6$ Hz, 2H), 5.83–5.74 (m, 1H), 5.59 (d, $J = 4.8$ Hz, 1H), 4.51 (d, $J = 5.2$ Hz, 1H), 3.86–3.78 (m, 1H), 3.75–3.68 (m, 1H), 3.65–3.55 (m, 1H), 3.19–3.11 (m, 1H), 2.95–2.87 (m, 1H), 2.70–2.63 (m, 2H), 2.59–2.48 (m, 1H), 2.29–2.12 (m, 2H), 2.09–2.02 (m, 1H), 1.99–1.90 (m, 2H), 1.88–1.75 (m, 3H), 1.71–1.64 (m, 2H), 1.63–1.57 (m, 2H), 1.48–1.34 (m, 1H), 1.14–0.97 (m, 2H). $^{13}\text{C-NMR}$ (101 MHz, CDCl_3) δ 165.3, 139.2, 134.8, 132.9, 129.2 (2), 128.7, 127.5 (2), 59.4, 59.2, 54.3, 46.7, 43.8, 40.6, 35.0, 31.3, 27.8, 26.2, 24.7, 24.4, 23.9, 19.1. ESI-HR-MS: calcd for $\text{C}_{23}\text{H}_{32}\text{N}_3\text{O}_3\text{S} [\text{M} + \text{H}]^+$: 430.2159, found: 430.2144.

12N-N'-m-Bromobenzenesulfonylaminoacetylaloperine (10d), Yield: 35%; white solid; m.p.: 101–103 °C. $^1\text{H-NMR}$ (400 MHz, CDCl_3) δ 8.02 (s, 1H), 7.82 (d, $J = 7.6$ Hz, 1H), 7.70 (d, $J = 8.0$ Hz, 1H), 7.39 (t, $J = 8.0$ Hz, 1H), 5.90–5.75 (m, 1H), 5.60 (d, $J = 5.2$ Hz, 1H), 4.53 (d, $J = 5.6$ Hz, 1H), 3.89–3.79 (m, 1H), 3.77–3.69 (m, 1H), 3.68–3.57 (m, 1H), 3.20–3.11 (m, 1H), 2.97–2.91 (m, 1H), 2.72–2.64 (m, 2H), 2.59–2.50 (m, 1H), 2.27–2.17 (m, 2H), 2.09–2.02 (m, 1H), 2.00–1.90 (m, 2H), 1.89–1.77 (m, 3H), 1.76–1.67 (m, 2H), 1.64–1.58 (m, 2H), 1.49–1.35 (m, 1H), 1.15–0.99 (m, 2H). $^{13}\text{C-NMR}$ (101 MHz, CDCl_3) δ 165.1, 141.2, 135.9, 134.7, 130.8, 130.4, 128.8, 126.1, 123.0, 59.5, 59.2, 54.3, 46.7, 43.8, 40.7, 35.0, 31.3, 27.8, 26.2, 24.7, 24.5, 23.9, 19.2. ESI-HR-MS: calcd for $\text{C}_{23}\text{H}_{31}\text{BrN}_3\text{O}_3\text{S} [\text{M} + \text{H}]^+$: 508.1264, found: 508.1249.

12N-N'-m-Trifluoromethylbenzenesulfonylaminoacetylaloperine (10e), Yield: 30%; white solid; m.p.: 91–93 °C. $^1\text{H-NMR}$ (400 MHz, CDCl_3) δ 8.15 (s, 1H), 8.08 (d, $J = 7.6$ Hz, 1H), 7.84 (d, $J = 7.6$ Hz, 1H), 7.67 (t, $J = 7.2$ Hz, 1H), 5.92 (s, 1H), 5.60 (s, 1H), 4.53 (d, $J = 4.4$ Hz, 1H), 3.92–3.82 (m, 1H), 3.80–3.70 (m, 1H), 3.68–3.57 (m, 1H), 3.28–3.10 (m, 1H), 3.05–2.87 (m, 1H), 2.71–2.60 (m, 1H), 2.59–2.50 (m, 1H), 2.28–2.13 (m, 2H), 2.08–2.00 (m, 1H), 1.99–1.88 (m, 2H), 1.88–1.75 (m, 3H), 1.75–1.66 (m, 2H), 1.65–1.56 (m, 3H), 1.47–1.37 (m, 1H), 1.13–0.99 (m, 2H). $^{13}\text{C-NMR}$ (101 MHz, CDCl_3) δ 165.0, 140.8, 134.6, 131.8, 130.8, 130.1, 129.5, 128.8, 124.5, 123.3, 59.5, 59.2, 54.3, 46.7, 43.9, 40.7, 34.9, 31.3, 27.7, 26.2, 24.7, 24.4, 23.9, 19.1. ESI-HR-MS: calcd for $\text{C}_{24}\text{H}_{31}\text{F}_3\text{N}_3\text{O}_3\text{S} [\text{M} + \text{H}]^+$: 498.2033, found: 498.2013.

12N-N'-m-Trifluoromethoxybenzenesulfonylaminoacetylaloperine (10f), Yield: 26%; white solid; m.p.: 81–83 °C. $^1\text{H-NMR}$ (400 MHz, CDCl_3) δ 7.83 (d, $J = 7.2$ Hz, 1H), 7.73 (s, 1H), 7.61–7.53 (m, 1H), 7.43 (d, $J = 8.0$ Hz, 1H), 5.93–5.76 (m, 1H), 5.61 (s, 1H), 4.54 (d, $J = 4.4$ Hz, 1H), 3.93–3.81 (m, 1H), 3.79–3.69 (m, 1H), 3.69–3.58 (m, 1H), 3.30–3.11 (m, 1H), 3.03–2.90 (m, 1H), 2.79–2.61 (m, 2H), 2.59–2.50 (m, 1H), 2.28–2.15 (m, 2H), 2.12–2.04 (m, 1H), 2.01–1.90 (m, 2H), 1.89–1.76 (m, 3H), 1.73–1.57 (m, 4H), 1.48–1.35 (m, 1H), 1.14–0.98 (m, 2H). $^{13}\text{C-NMR}$ (101 MHz, CDCl_3) δ 165.1, 149.4, 141.6, 134.7, 131.0, 128.8, 125.7, 125.1, 120.4, 120.1, 59.5, 59.1, 54.4, 46.7, 43.9, 40.7, 34.8, 31.3, 27.7, 26.2, 24.7, 24.4, 23.9, 19.1. ESI-HR-MS: calcd for $\text{C}_{24}\text{H}_{31}\text{F}_3\text{N}_3\text{O}_4\text{S} [\text{M} + \text{H}]^+$: 514.1982, found: 514.1967.

12N-N'-(3,5-Difluoromethyl)benzenesulfonylaminoacetylaloperine (10g), Yield: 22%; brown solid; m.p.: 78–80 °C. $^1\text{H-NMR}$ (400 MHz, CDCl_3) δ 8.33 (s, 2H), 8.06 (s, 1H), 6.05 (s, 1H), 5.61 (d, $J = 4.8$ Hz, 1H), 4.55 (d, $J = 5.2$ Hz, 1H), 4.01–3.86 (m, 1H), 3.83–3.75 (m, 1H), 3.73–3.60 (m, 1H), 3.22–3.10 (m, 1H), 3.04–2.91 (m, 1H), 2.76–2.61 (m, 2H), 2.59–2.47 (m, 1H), 2.27–2.17 (m, 2H), 2.07–2.01 (m, 1H), 2.00–1.90 (m, 2H), 1.89–1.77 (m, 3H), 1.76–1.68 (m, 2H), 1.64 (s, 1H), 1.60 (s, 1H), 1.44–1.39 (m, 1H), 1.14–0.99 (m, 2H). $^{13}\text{C-NMR}$ (101 MHz, CDCl_3) δ 164.8, 142.7, 134.6, 132.9 (2), 127.7 (2), 126.3 (2), 122.6 (2), 59.6, 59.2, 54.3, 46.6, 43.9, 40.8, 34.9, 31.2, 27.7, 26.2, 24.7, 24.4, 23.9, 19.1. ESI-HR-MS: calcd for $\text{C}_{25}\text{H}_{30}\text{F}_6\text{N}_3\text{O}_3\text{S} [\text{M} + \text{H}]^+$: 566.1907, found: 566.1897.

3.3. Biology Assay

3.3.1. Cell Culture and Screening of Compounds

Cells were maintained on Dulbecco's Modified Eagle's medium (DMEM), laid on 96-well plate. DMEM medium was supplemented with 10% fetal bovine serum (FBS) at 37 °C humidified atmosphere

with 5% CO₂. Furthermore, serum-free culture was required until the cells were confluent at 90–95%. 24 h later the cells were treated with a tested compound (40 and 80 µM) for 24 h. The COL1A1 promoter activity was detected by the Bright-Glo luciferase assay system. Alternatively, to test the acute effects of compound on luciferase activity, 24 h later the cells were lysed and the lysate was treated with a tested compound (80 µM) for 2 h, then the luciferase was detected by the Bright-Glo luciferase assay system (Promega, Madison, WI, USA).

3.3.2. Cell Survival Assay

HepG2 cell survival was measured by MTT assay. HepG2 cells, at density of 6×10^3 cells/well in 96-well culture plates, were incubated with the aloperine derivatives at various concentrations until the cells at 50% confluence for 24 h. 20 µL of the MTT (5 mg/mL) solution was added to each plate and incubated with 5% CO₂, 37 °C for 4 h. Subsequently, withdrawing the culture supernatant containing MTT, 150 µL DMSO was used for dissolving the formazan crystal. The absorbance was measured using a microplate reader at 570 nm.

LX-2 cell survival was measured by sulforhodamine B (SRB) assay. The cells were seeded in 96-well plates at the density of 2×10^4 /well and cultured in DMEM/GlutaMAX I medium with 10% fetal bovine serum (FBS) with 5% CO₂, 37 °C. The cells were treated by the aloperine derivatives for 24 h, washed by PBS for three times. Then the cells were fixed with 10% (*wt/vol*) trichloroacetic acid for 1 h and stained with SRB for 0.5 h. Subsequently, the protein-bound dye was dissolved in 10 mM Tris base solution after removing excess SRB dye washing repeatedly with 1% (*vol/vol*) acetic acid, the optical density (OD) was determined at 510 nm with a microplate reader.

3.3.3. RT-qPCR Assay

LX-2 cells were laid on 6-well plate and cultured in DMEM supplemented with 10% fetal bovine serum (FBS) in a 5% CO₂ atmosphere at 37 °C. And serum-free culture was required until the cells reached 90–95% confluence. After 24 h, cells were incubated with 40 and 80 µM concentrations of aloperine derivatives in the presence of 2 ng/mL of TGF-β1 for 24 h. Total RNA of the LX-2 cells was isolated using TRIzol reagent, purified using NucleoSpin RNA Clean-up. Reverse transcription was performed with Transcriptor first strand cDNA synthesis kit. Subsequently, the cDNA levels was determined by ABI 7500 Fast Real-Time PCR System using TaqMan probes of COL1A1, TGF-β1, α-SMA, and GAPDH (sequence not disclosed by ABI) and FastStart Universal Probe master mix (Roche, Indianapolis, IN, USA).

3.3.4. Western Blot

LX-2 cells were cultured as described above. Cells were washed with phosphate-buffered saline (PBS) and were resuspended by radioimmunoprecipitation assay (RIPA) lysis buffer for 30 min in 4 °C; the supernatant was collected after centrifugation at 12000 g for 15 min at 4 °C. Subsequently, equal amounts of protein were quantified with Bradford assay, separated using SDS-PAGE and transferred onto polyvinylidene difluoride membrane. The membranes were blocked with 5% milk in PBST for 1 h, and probed with specific primary antibodies overnight at room temperature. The membrane was washed three times by PBST, and probed with horseradish peroxidase-conjugated secondary antibodies and GAPDH. The proteins were visualized by chemiluminescence reagents. Antibodies used in western blot analysis were obtained from Abcam (Cambridge, UK): anti-collagen 1 (ab34710), anti-TGF beta 1 antibody (ab179695), anti-alpha smooth muscle actin (ab32575) and Cell Signaling Technology (Danvers, MA, USA): GAPDH (D16H11) Rabbit mAb (5174).

3.3.5. Statistics

Results are presented as mean values ± standard error of independent triplicate experiments. All statistical analyses were performed by using two-tailed Student's t-test and *p*-values of less than 0.05 were considered statistically significant.

3.4. Acute Toxicity

Male and Female Kunming mice with weight of 20.0 ± 1.0 g were obtained from the Institute of Laboratory Animal Science (Beijing, China). Animals were cared according to the institutional guidelines of the Institute of Medicinal Biotechnology, CAMS&PUMC (IMB-20190610D3), and fed with regular rodent chow and housed in an air conditioned room. The mice were randomly divided into different groups with four male mice and four female mice each. Each compound was given orally in a single-dosing experiment, the dose of **4i** was 100, 300 and 400 mg kg⁻¹, the dose of **4n** was 300, 400, 500 mg kg⁻¹, the dose of **4p** was 200, 400, 500 mg kg⁻¹ (ddH₂O as control). The mice were closely monitored for 7 days. Body weight as well as survival was monitored.

4. Conclusions

To conclude, twenty seven new aloperine derivatives with a unique endocyclic scaffold were designed, synthesized and evaluated for their inhibitory effect on COL1A1 promotor in LX2 cells, taking **1** as the lead. The SAR results indicated that the introduction of suitable substituents on the 12N atom might be beneficial for activity. Compound **4p** exhibited good potency on COL1A1 promotor with an IC₅₀ value of 16.5 μM. Its inhibitory activity against COL1A1 was further confirmed at both the mRNA and protein levels. Meanwhile, it effectively inhibited the expression of fibrogenic proteins, such as α-SMA and TGF-β1, indicating the promise against liver fibrogenesis. It also exhibited a good in vivo safety profile, with an LD₅₀ value of 400 mg kg⁻¹ in mice via intragastrical administration. Overall, this study initiated the anti-COL1A1 SAR of aloperine derivatives, and thus gave useful information for further developing these compounds into promising anti-liver fibrogenesis candidates with a unique endocyclic scaffold, and compound **4p** has been chosen as the lead for the further research.

Supplementary Materials: The following are available online, Figure S1: The acute effects on luciferase activity of target compounds. Figure S2: The IC₅₀ bar graphs of target compounds. Figure S3: The cell viability of target compounds in LX-2 cells. Figure S4: The cell viability of target compounds in HepG2 cells. Table S1: P values of the RT-PCR of target compounds in Figure 2. Table S2: P values of the western blot intensity of target compounds in Figure 3.

Author Contributions: K.W. performed the synthetic experiments and wrote the paper, Z.G. performed the synthetic experiments, Y.B. performed the biological assay and drew the graphics, Y.P. searched the literatures, Y.L. revised the paper, conceived the chemistry experiments and provided the funding support, H.H. conceived the biological experiments, D.S. revised the manuscript and provided the funding support. All authors have read and agreed to the published version of the manuscript.

Funding: This work was supported by CAMS initiative for innovative medicine (2017-12M-3-012), the Beijing Natural Science Foundation (7202131) and Chinese Pharmaceutical Association-Yiling Pharmaceutical Innovation Fund for Biomedicine (GL-1-B04-20190397).

Acknowledgments: The authors thank center for analysis and testing of Institute of Materia Medica, Chinese Academy of Medical Sciences for their contributions to the determination of ¹H-NMR and ¹³C-NMR, and center for analysis and testing of Institute of Medicinal Biotechnology, Chinese Academy of Medical Sciences for their contributions to the determination of HRMS.

Conflicts of Interest: The authors declare no conflict of interest.

References

1. Lee, Y.A.; Wallace, M.C.; Friedman, S.L. Pathobiology of liver fibrosis: A translational success story. *Gut* **2015**, *64*, 830–841. [[CrossRef](#)] [[PubMed](#)]
2. Tsuchida, T.; Friedman, S.L. Mechanisms of hepatic stellate cell activation. *Nat. Rev. Gastroenterol. Hepatol.* **2017**, *14*, 397–411. [[CrossRef](#)] [[PubMed](#)]
3. Rinella, M.E.; Sanyal, A.J. Management of NAFLD: A stage-based approach. *Nat. Rev. Gastroenterol. Hepatol.* **2016**, *13*, 196–205. [[CrossRef](#)] [[PubMed](#)]
4. Ebrahimi, H.; Naderian, M.; Sohrabpour, A.A. New Concepts on Reversibility and Targeting of Liver Fibrosis; A Review Article. *Middle East J. Dig. Dis.* **2018**, *10*, 133–148. [[CrossRef](#)] [[PubMed](#)]

5. Sun, M.; Kisseleva, T. Reversibility of liver fibrosis. *Clin. Res. Hepatol. Gastroenterol.* **2015**, *39*, S60–S63. [[CrossRef](#)]
6. Jin, X.; Aimaiti, Y.; Chen, Z.; Wang, W.; Li, D. Hepatic stellate cells promote angiogenesis via the TGF-beta1-Jagged1/VEGFA axis. *Exp. Cell Res.* **2018**, *373*, 34–43. [[CrossRef](#)]
7. Carson, J.P.; Ramm, G.A.; Robinson, M.W.; McManus, D.P.; Gobert, G.N. Schistosome-Induced Fibrotic Disease: The Role of Hepatic Stellate Cells. *Trends Parasitol.* **2018**, *34*, 524–540. [[CrossRef](#)]
8. Ghafoory, S.; Varshney, R.; Robison, T.; Kouzbari, K.; Woolington, S.; Murphy, B.; Xia, L.; Ahamed, J. Platelet TGF-β1 deficiency decreases liver fibrosis in a mouse model of liver injury. *Blood Adv.* **2018**, *2*, 470–480. [[CrossRef](#)]
9. Tang, L.Y.; Heller, M.; Meng, Z.; Yu, L.R.; Tang, Y.; Zhou, M.; Zhang, Y.E. Transforming Growth Factor-beta (TGF-beta) Directly Activates the JAK1-STAT3 Axis to Induce Hepatic Fibrosis in Coordination with the SMAD Pathway. *J. Biol. Chem.* **2017**, *292*, 4302–4312. [[CrossRef](#)]
10. Phaosri, M.; Jantrapirom, S.; Takuathung, M.N.; Soonthornchareonnon, N.; Sireeratawong, S.; Buacheen, P.; Pitchakarn, P.; Nimlamool, W.; Potikanond, S. *Salacia chinensis* L. Stem Extract Exerts Antifibrotic Effects on Human Hepatic Stellate Cells Through the Inhibition of the TGF-beta1-Induced SMAD2/3 Signaling Pathway. *Int. J. Mol. Sci.* **2019**, *20*, 6314. [[CrossRef](#)]
11. Friedman, S.L. Hepatic stellate cells: Protean, multifunctional, and enigmatic cells of the liver. *Physiol. Rev.* **2008**, *88*, 125–172. [[CrossRef](#)]
12. Yanguas, S.C.; Cogliati, B.; Willebrords, J.; Maes, M.; Colle, I.; van den Bossche, B.; de Oliveira, C.P.M.S.; Andraus, W.; Alves, V.A.F.; Leclercq, I.; et al. Experimental models of liver fibrosis. *Arch. Toxicol.* **2016**, *90*, 1025–1048. [[CrossRef](#)] [[PubMed](#)]
13. Zhao, S.S.; Wang, J.X.; Wang, Y.C.; Shao, R.G.; He, H.W. Establishment and application of a high-throughput drug screening model based on COL1A1 promoter for anti-liver fibrosis. *Acta Pharmaceutica Sinica* **2015**, *50*, 169–173. [[PubMed](#)]
14. Ge, M.; Liu, H.; Zhang, Y.; Li, N.; Zhao, S.; Zhao, W.; Zhen, Y.; Yu, J.; He, H.; Shao, R.G. The anti-hepatic fibrosis effects of dihydrotanshinone I are mediated by disrupting the yes-associated protein and transcriptional enhancer factor D2 complex and stimulating autophagy. *Br. J. Pharmacol.* **2017**, *174*, 1147–1160. [[CrossRef](#)]
15. Tang, S.; Li, Y.; Bao, Y.; Dai, Z.; Niu, T.; Wang, K.; He, H.; Song, D. Novel cytosine derivatives exert anti-liver fibrosis effect via PI3K/Akt/Smad pathway. *Bioorg. Chem.* **2019**, *90*, 103032. [[CrossRef](#)] [[PubMed](#)]
16. Niu, T.; Niu, W.; Bao, Y.; Liu, T.; Song, D.; Li, Y.; He, H. Discovery of Matrinic Thiadiazole Derivatives as a Novel Family of Anti-Liver Fibrosis Agents via Repression of the TGFbeta/Smad Pathway. *Molecules* **2018**, *23*, 1644. [[CrossRef](#)]
17. Xu, Z.; Wang, X.; Chen, X.; Zeng, S.; Qian, L.; Wei, J.; Gong, Z.; Yan, Y. Identification of Aloperine as an anti-apoptotic Bcl2 protein inhibitor in glioma cells. *PeerJ.* **2019**, *7*, e7652. [[CrossRef](#)]
18. Muhammad, T.; Sakhawat, A.; Khan, A.A.; Huang, H.; Khan, H.R.; Huang, Y.; Wang, J. Aloperine in combination with therapeutic adenoviral vector synergistically suppressed the growth of non-small cell lung cancer. *J. Cancer Res. Clin. Oncol.* **2020**, *146*, 861–874. [[CrossRef](#)] [[PubMed](#)]
19. Wang, C.; Choi, Y.H.; Xian, Z.; Zheng, M.; Piao, H.; Yan, G. Aloperine suppresses allergic airway inflammation through NF-kappaB, MAPK, and Nrf2/HO-1 signaling pathways in mice. *Int. Immunopharmacol.* **2018**, *65*, 571–579. [[CrossRef](#)]
20. Zhang, X.; Lv, X.Q.; Tang, S.; Mei, L.; Li, Y.H.; Zhang, J.P.; Jiang, J.D.; Peng, Z.G.; Song, D.Q. Discovery and evolution of aloperine derivatives as a new family of HCV inhibitors with novel mechanism. *Eur. J. Med. Chem.* **2018**, *143*, 1053–1065. [[CrossRef](#)]
21. Zhang, X.; Liu, Q.; Zhang, N.; Li, Q.Q.; Liu, Z.D.; Li, Y.H.; Gao, L.M.; Wang, Y.C.; Deng, H.B.; Song, D.Q. Discovery and evolution of aloperine derivatives as novel anti-filovirus agents through targeting entry stage. *Eur. J. Med. Chem.* **2018**, *149*, 45–55. [[CrossRef](#)]
22. Yin, W.; Han, J.; Zhang, Z.; Han, Z.; Wang, S. Aloperine Protects Mice against Bleomycin-induced Pulmonary Fibrosis by Attenuating Fibroblast Proliferation and Differentiation. *Sci. Rep.* **2018**, *8*, 6265. [[CrossRef](#)] [[PubMed](#)]
23. Yu, D.K.; Zhang, C.X.; Zhao, S.S.; Zhang, S.H.; Zhang, H.; Cai, S.Y.; Shao, R.G.; He, H.W. The anti-fibrotic effects of epigallocatechin-3-gallate in bile duct-ligated cholestatic rats and human hepatic stellate LX-2 cells are mediated by the PI3K/Akt/Smad pathway. *Acta Pharmacol. Sin.* **2015**, *36*, 473–482. [[CrossRef](#)] [[PubMed](#)]

24. Song, Q.H.; Klepeis, V.E.; Nugent, M.A.; Trinkaus-Randall, V. TGF-beta1 regulates TGF-beta1 and FGF-2 mRNA expression during fibroblast wound healing. *Mol Pathol.* **2002**, *55*, 164–176. [[CrossRef](#)] [[PubMed](#)]
25. Krizhanovsky, V.; Yon, M.; Dickins, R.A.; Hearn, S.; Simon, J.; Miething, C.; Yee, H.; Zender, L.; Lowe, S.W. Senescence of activated stellate cells limits liver fibrosis. *Cell* **2008**, *134*, 657–667. [[CrossRef](#)]
26. Dattaroy, D.; Pourhoseini, S.; Das, S.; Alhasson, F.; Seth, R.K.; Nagarkatti, M.; Michelotti, G.A.; Diehl, A.M.; Chatterjee, S. Micro-RNA 21 inhibition of SMAD7 enhances fibrogenesis via leptin-mediated NADPH oxidase in experimental and human nonalcoholic steatohepatitis. *Am. J. Physiol. Gastrointest. Liver Physiol.* **2015**, *308*, G298–G312. [[CrossRef](#)]
27. Stefanovic, B.; Stefanovic, L. Screening for antifibrotic compounds using high throughput system based on fluorescence polarization. *Biology* **2014**, *3*, 281–294. [[CrossRef](#)]

Sample Availability: Samples of the compounds 4a–p, 7a–d and 10a–g are available from the authors.

Publisher’s Note: MDPI stays neutral with regard to jurisdictional claims in published maps and institutional affiliations.



© 2020 by the authors. Licensee MDPI, Basel, Switzerland. This article is an open access article distributed under the terms and conditions of the Creative Commons Attribution (CC BY) license (<http://creativecommons.org/licenses/by/4.0/>).